Clinical Cancer Research

Long Noncoding RNA *LBCS* Inhibits Self-Renewal and Chemoresistance of Bladder Cancer Stem Cells through Epigenetic Silencing of SOX2

Xu Chen[1,2], Ruihui Xie[1,2], Peng Gu[1], Ming Huang[1,2], Jinli Han[1], Wen Dong[1], Weibin Xie[1,2], Bo Wang[1,2], Wang He[1], Guangzheng Zhong[1], Ziyue Chen[3], Jian Huang[1], and Tianxin Lin[1,2]

Abstract

Purpose: Chemoresistance and tumor relapse are the leading cause of deaths in bladder cancer patients. Bladder cancer stem cells (BCSCs) have been reported to contribute to these pathologic properties. However, the molecular mechanisms underlying their self-renewal and chemoresistance remain largely unknown. In the current study, a novel lncRNA termed Low expressed in Bladder Cancer Stem cells (*lnc-LBCS*) has been identified and explored in BCSCs.

Experimental Design: Firstly, we establish BCSCs model and explore the BCSCs-associated lncRNAs by transcriptome microarray. The expression and clinical features of *lnc-LBCS* are analyzed in three independent large-scale cohorts. The functional role and mechanism of *lnc-LBCS* are further investigated by gain- and loss-of-function assays *in vitro* and *in vivo*.

Results: *Lnc-LBCS* is significantly downregulated in BCSCs and cancer tissues, and correlates with tumor grade, chemotherapy response, and prognosis. Moreover, *lnc-LBCS* markedly inhibits self-renewal, chemoresistance, and tumor initiation of BCSCs both *in vitro* and *in vivo*. Mechanistically, *lnc-LBCS* directly binds to heterogeneous nuclear ribonucleoprotein K (hnRNPK) and enhancer of zeste homolog 2 (EZH2), and serves as a scaffold to induce the formation of this complex to repress SRY-box 2 (SOX2) transcription via mediating histone H3 lysine 27 tri-methylation. SOX2 is essential for self-renewal and chemoresistance of BCSCs, and correlates with the clinical severity and prognosis of bladder cancer patients.

Conclusions: As a novel regulator, *lnc-LBCS* plays an important tumor-suppressor role in BCSCs' self-renewal and chemoresistance, contributing to weak tumorigenesis and enhanced chemosensitivity. The *lnc-LBCS*–hnRNPK–EZH2–SOX2 regulatory axis may represent a therapeutic target for clinical intervention in chemoresistant bladder cancer.

Introduction

With a high rate of recurrence and tumor heterogeneity, bladder cancer is one of the most common and lethal malignancies worldwide (1, 2). Chemotherapy is a significant component of current first-line treatment for bladder cancer. It reduces tumor masses in most patients initially; however, a majority of patients progressively become unresponsive after multiple treatment cycles, and ultimately suffer tumor relapse (3, 4). Recent studies demonstrate that the main cause of chemoresistance is existence of cancer stem cells (CSCs), which have a survival advantage in response to chemotherapy (4, 5). Therefore, CSCs are responsible for the initiation, propagation, metastasis, chemoresistance, and relapse of cancers (3, 5, 6). Previous studies have verified the existence of bladder cancer stem cells (BCSCs; refs. 7, 8), which can be distinguished by various biomarkers and particular characteristics, such as CD44 (7), high aldehyde dehydrogenase (ALDH) activity (9), and sphere formation (10). Given the critical role of CSCs in tumorigenesis, intervention to block CSCs' self-renewal could be a potential strategy for tumor treatment. However, the biological characters and molecular mechanisms of chemotherapy-induced BCSCs remain largely unknown.

Long noncoding RNAs (lncRNA) are transcripts longer than 200 nucleotides without protein-coding capacity (11). Accumulating evidence indicates that lncRNAs are involved in diverse physiologic and pathologic progresses, including embryonic development, organ formation, and tumorigenesis (12, 13). Aberrant expression of lncRNAs has been observed in many types of cancers and may play important roles in regulating proliferation, chemoresistance, and metastasis of cancer cells (14, 15). Recent studies show that lncRNAs are key regulators of self-renewal in CSCs of liver, renal, and colon cancer, such as lncTCF7 (16), lncARSR (17), and RBM5-AS1 (18). However, whether and how lncRNAs regulate the self-renewal and chemoresistance of BCSCs remains largely unknown.

In the present study, we discovered a novel lncRNA termed Low expressed in Bladder Cancer Stem cells (*lnc-LBCS*), which is

[1]Department of Urology, Sun Yat-sen Memorial Hospital, Sun Yat-sen University, Guangzhou, China. [2]Guangdong Provincial Key Laboratory of Malignant Tumor Epigenetics and Gene Regulation, Sun Yat-Sen Memorial Hospital, Sun Yat-Sen University, Guangzhou, China. [3]Department of Pediatric Surgery, Sun Yat-sen Memorial Hospital, Sun Yat-sen University, Guangzhou, China.

Note: Supplementary data for this article are available at Clinical Cancer Research Online (http://clincancerres.aacrjournals.org/).

X. Chen, R. Xie, and P. Gu contributed equally to this article.

Corresponding Authors: Tianxin Lin, Sun Yat-sen Memorial Hospital, Sun Yat-sen University, Guangzhou, Guangdong 510120, China. Phone: 86-020-34070447; Fax: 86-20-81332336; E-mail: lintx@mail.sysu.edu.cn; and Jian Huang, Phone: 86-13600054833; Fax: 86-20-81332336; E-mail: urolhj@sina.com

doi: 10.1158/1078-0432.CCR-18-1656

Translational Relevance

Tumor chemoresistance and subsequent recurrence remain a core challenge in the clinical intervention of bladder cancer. Cancer stem cells (CSCs) have been demonstrated to be implicated in the tumor initiation, drug resistance, and relapse. However, the mechanism in which CSCs mediated chemoresistance and recurrence remains largely unknown. In this study, we identified a novel bladder cancer stem cells (BCSCs)–associated long noncoding RNA (lncRNA) termed *LBCS*, which is markedly downregulated in BCSCs and cancer tissues, and significantly associated with tumor grade, chemotherapy response, and prognosis in bladder cancer patients. Furthermore, we found that *lnc-LBCS* promoted the chemosensitivity of bladder cancer through inhibition of BCSCs' self-renewal via guiding the heterogeneous nuclear ribonucleoprotein K (hnRNPK)–enhancer of zeste homolog 2 (EZH2) complex to epigenetic repression of SOX2. We firstly demonstrate the critical role of *lnc-LBCS*–hnRNPK–EZH2–SOX2 axis in BCSCs. Our findings may provide a potential new target for bladder cancer diagnosis and therapy.

significantly downregulated in BCSCs and inhibits self-renewal and chemoresistance of BCSCs *in vitro* and *in vivo*. Interestingly, *lnc-LBCS* guides heterogeneous nuclear ribonucleoprotein K (hnRNPK)–enhancer of zeste homolog 2 (EZH2) complex to suppress SOX2 expression by mediating H3K27me3 of SOX2 promoter, leading to inhibition of BCSCs' self-renewal and chemoresistance.

Materials and Methods

Cell cultures

The human bladder cancer cell lines (UM-UC-3, 5637, HT-1376, and J82) and human embryonic kidney (HEK-293T) cells were purchased from the American Type Culture Collection from 2013 to 2015. UM-UC-3, HT-1376, J82, and HEK-293T cells were cultured in DMEM (Gibco), whereas 5637 cells were cultured in RPMI 1640 (Gibco). All medium was supplemented with 10% FBS (Shanghai ExCell Biology) and 1% penicillin/streptomycin (Gibco). Cells were cultured in a humidified atmosphere of 5% CO_2 at 37°C. These cells were characterized using short tandem repeat markers and were confirmed to be mycoplasma-free (last tested in 2018).

Human tissue samples

A total of 120 pair snap-frozen fresh bladder cancer tissues and normal adjacent tissues (NAT), termed Cohort 1, were obtained by surgery with the written consent of patients who underwent surgery at Sun Yat-sen Memorial Hospital, Sun Yat-sen University. The workflow of patients was selected in Cohort 1 (Supplementary Fig. S17). Three tissue microarrays containing 86 bladder cancer specimens and 20 normal tissues, termed Cohort 2, were purchased from US Biomax (catalogue numbers BL244, BC12011b, and T124b). All the samples were pathologically confirmed as transitional cell carcinoma of the bladder by two pathologists. Ethical consent was approved by Sun Yat-sen University's Committees for Ethical Review of Research involving Human Subjects. The study was conducted in accordance with the International Ethical Guidelines for Biomedical Research Involving Human Subjects (CIOMS). The characteristics and clinicopathologic features of the patients are listed in Supplementary Table S1.

Mouse xenograft experiments

All animal studies were conducted with the approval of the Sun Yat-sen University Institutional Animal Care and Use Committee and were performed in accordance with established guidelines. Male BALB/c nude mice (4–5 weeks old) were purchased from the Experimental Animal Center of Sun Yat-sen University and housed in SPF barrier facilities. The tumor-initiating capacity assay and *in vivo* chemotherapy assay were detailed in the Supplementary Materials and Methods section. The size of the tumor was measured every 3 days. The mice were euthanized, and tumors were dissected surgically at the end of experiment. The tumor specimens were fixed in 4% paraformaldehyde.

Microarray analysis

The LncRNA+mRNA Human Gene Expression Microarray (CapitalBio) was used to investigate the differentially expressed lncRNAs in UM-UC-3 4th spheres, spheres readhered for 10 hours, and 1 day, and adherent UM-UC-3 cells. All primary data in the microarray analysis have been uploaded to the Gene Expression Omnibus with the accession number GSE107857.

The Cancer Genome Atlas data mining

Patients' clinical profiles in The Cancer Genome Atlas (TCGA) bladder cancer cohort are available at https://cancergenome.nih.gov/ (19). The expression of the TCGA *lnc-LBCS* cohort comprising 209 patients was obtained from TANRIC (ref. 20; http://ibl.mdanderson.org/tanric/_design/basic/query.html), but patients with no available clinical data were excluded from the analysis. So a total of 185 patients were used for further analysis. The characteristics and clinicopathologic features of the patients are listed in Supplementary Table S1. For the overall survival (OS) and disease-free survival (DFS) analysis, the Kaplan–Meier survival analysis of SOX2 in 402 cases in a TCGA cohort was obtained from GEPIA (ref. 21; http://gepia.cancer-pku.cn/index.html).

Sphere culture and Aldefluor assay

Sphere culture was conducted as previously described (22, 23) and as detailed in the Supplementary Materials and Methods section. Cells were assayed for ALDH activity using the Aldefluor Kit (Stem Cell Technologies) according to the manufacturer's instructions.

Chemosensitivity assay, apoptosis analysis, detection of caspase-3/7 activity, and the terminal deoxynucleotidyl transferase–mediated dUTP nick end labeling assay

The chemosensitivity assay and apoptosis analysis were performed as described previously (23–25) and as detailed in the Supplementary Materials and Methods section. Caspase-3/7 activity was measured using a Caspase-Glo 3/7 Assay kit (Promega) as previously described (23, 24). The terminal deoxynucleotidyl transferase–mediated dUTP nick end labeling (TUNEL) assay was conducted using the *In Situ* Cell Death Detection Kit (Roche), following the manufacturer's instructions and as described previously (25).

ISH and IHC

Lnc-LBCS expression was also examined using ISH in formalin-fixed, paraffin-embedded (FFPE) samples, as previously described (26) and as detailed in the Supplementary Materials and Methods section. The IHC analyses and score calculation were conducted as described previously (23, 24). Anti-SOX2 antibodies (1:500) were used to detect the expression of SOX2 in bladder cancer tissues. The expression of *lnc-LBCS* and SOX2 in bladder specimens was quantified by using the histochemical score (H-score) as described previously (23, 24). The staining intensity was graded as follows: 0 (no staining), 1 (weak staining, light yellow for IHC, light blue for ISH), 2 (moderate staining, brown for IHC, moderate blue for ISH), and 3 (strong staining, brown red for IHC, strong blue for ISH). The intensity of staining was multiplied by the percentage of positive cells (0%–100%), and the H-score (0–300) of each tissue was obtained for statistical analysis. The samples were classed as low (score < 50) or high (score $\geq$ 50) *lnc-LBCS* expression. The samples were classed as low (score < 200) or high (score $\geq$ 200) SOX2 expression. Anti-Ki67 antibodies (1:1,000) were used to detect the expression of Ki67 in mouse tumors. The score of ISH and IHC in the FFPE samples was blindly quantified by two pathologists, and the average H-score (0–300) of each tissue was obtained for statistical analysis.

RNA isolation, qRT-PCR, and Western blotting

RNA isolation and qRT-PCR were performed as previously described (25, 27). Relative expression was calculated using the $2^{-\Delta\Delta Ct}$ method (Ct, cycle threshold). All specific primers are listed in Supplementary Table S10. Western blotting was performed as previously described (25, 27). The information of antibody was detail in the Supplementary Materials and Methods section. The full images of all Western blots are shown in Supplementary Figs. S18 and S19.

RNA pulldown and RNA-binding protein immunoprecipitation assay

Lnc-LBCS full-length sense, antisense, and serial deletion sequences were prepared via *in vitro* transcription using a TranscriptAid T7 High Yield Transcription Kit. The RNA pulldown assay was performed using a Magnetic RNA-Protein Pull-down kit according to the manufacturer's instructions. The samples were separated using electrophoresis, and *lnc-LBCS*–specific bands were identified using mass spectrometry and retrieved from a human proteome library. The RIP was performed as described previously (25) and as detailed in the Supplementary Materials and Methods section.

Chromatin isolation by RNA purification and chromatin immunoprecipitation assay

The chromatin isolation by RNA purification (ChIRP) was conducted using a Magna ChIRP RNA Interactome kit (Millipore) according to the manufacturer's instructions and as described previously (25). Chromatin immunoprecipitation (ChIP) was conducted using an EZ-Magna ChIP A/G kit (Millipore) according to the manufacturer's instructions and as previously reported (23–25). The method of ChIRP and ChIP was detail in the Supplementary Materials and Methods section.

Statistical analyses

Quantitative data were presented as the mean ± the SD of three independent experiments. Differences between two groups were analyzed with the unpaired/paired Student *t* test (two-tailed tests), and one-way ANOVA followed by Dunnett multiple comparisons tests was performed when more than two groups were compared. Data of clinical analysis were shown as median with the interquartile range. The Mann–Whitney *U* test was used for independent samples when the population could not be assumed to be normally distributed. Pearson χ^2 test was used to analyze the clinical variables. Spearman correlation analysis was performed to determine the correlation between two variables. Cumulative survival time was calculated using the Kaplan–Meier method and analyzed by the log-rank test. The best point cutoff value was used to define *lnc-LBCS* expression level (low vs. high) for all survival analyses in this study. A multivariate Cox proportional hazards model was used to estimate the adjusted HRs and 95% confidence intervals, and to identify independent prognostic factors. All statistical analyses in this study were performed using SPSS 19.0 software. A P value < 0.05 was considered significant.

Results

BCSCs are enriched under pressure from chemotherapy

Previous studies have demonstrated that CSCs, such as breast and bladder CSCs, are selectively enriched after chemotherapy via enhanced survival (4, 28). We took advantage of this finding to determine if we could enrich BCSCs by consecutively passaging bladder cancer cells in NOD/SCID mice treated with chemotherapy. We obtained the cells termed UM-UC-3 4th from four chemotherapy passages *in vivo* (Supplementary Fig. S1A). To study whether UM-UC-3 4th cells were resistant to chemotherapy, we performed MTT assays, flow cytometry, and caspase-3/7 activity assays in UM-UC-3 4th and parental UM-UC-3 cells. Notably, UM-UC-3 4th cells displayed higher chemotherapy resistance and a higher IC_{50} value, and a lower apoptosis rate and caspase-3/7 activity than the parental UM-UC-3 cells when treated with gemcitabine or cisplatin (Supplementary Fig. S1B–S1D). This suggested that UM-UC-3 4th cells were chemoresistant bladder cancer cells.

To evaluate whether UM-UC-3 4th cells had a stronger self-renewal capacity, we performed a sphere formation assay *in vitro* and a tumor initiation assay *in vivo*. UM-UC-3 4th cells formed more and larger spheres than UM-UC-3 cells (Supplementary Fig. S1E and S1F). A serial sphere formation assay showed that UM-UC-3 4th cells had a stronger long-term self-renewal over four generations of sphere formation compared with UM-UC-3 cells (Supplementary Fig. S1G). Tumor initiation assay showed that UM-UC-3 4th cells had a stronger tumorigenic capacity and contained remarkably higher ratios of BCSCs than parental UM-UC-3 cells (Supplementary Fig. S1H–S1J). Furthermore, UM-UC-3 4th-formed spheres contained more $ALDH^+$ cells, a functional marker of BCSCs, and increased expression of OCT4, SOX2, and NANOG, which are key stem cells markers (Supplementary Fig. S1K and S1L). Therefore, we used the UM-UC-3 4th spheres as BCSCs for further study.

Lnc-LBCS is markedly downregulated in BCSCs

To identify lncRNAs involved in BCSCs, we conducted a transcriptome microarray analysis of UM-UC-3 4th spheres,

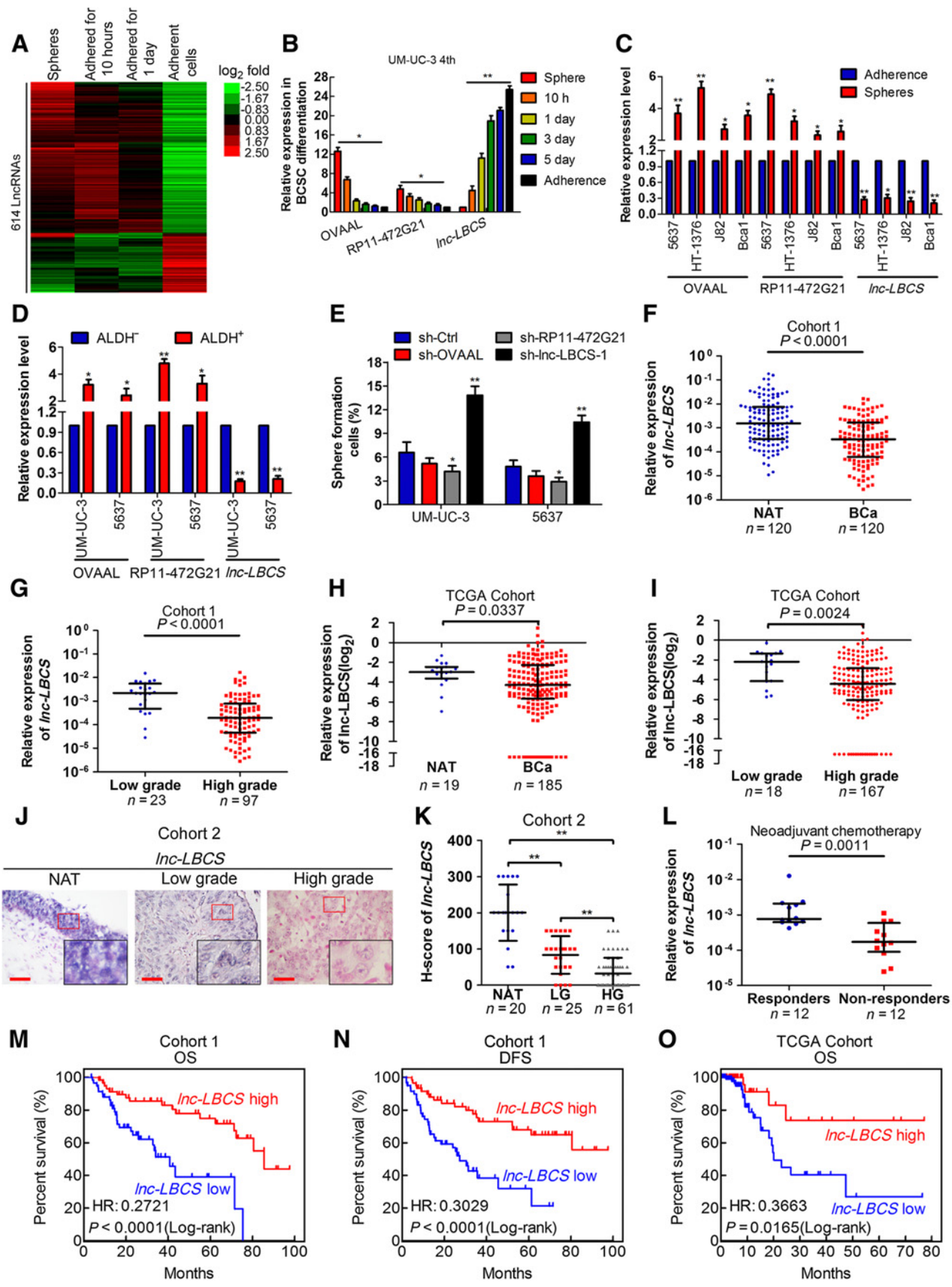

spheres readhered for 10 hours, 1 day, and adherent UM-UC-3 cells. As shown in Fig. 1A, 614 lncRNAs decreased or increased in UM-UC-3 4th spheres compared with readhered spheres, including CASC2 (29), XIST (30), and OVAAL (31), which are associated with human cancer progression. We then further examined the expression of 5 most decreased lncRNAs and 5 most increased lncRNAs in a series of BCSCs models, including UM-UC-3 4th spheres differentiation, four other bladder cancer spheres, UM-UC-3, and 5637 $ALDH^+$ cells. The expression levels of three lncRNAs were closely correlated with a series of BCSCs' models (Fig. 1B–D). Moreover, sphere formation assay was performed to identify which lncRNA plays a key role in self-renewal of BCSCs using lentivirus-mediated shRNAs (Supplementary Fig. S2A). Finally, we identified a novel lncRNA (ENSG00000228412), termed *lnc-LBCS*, that was significantly downregulated in BCSCs and affected sphere formation (Fig. 1E).

Lnc-LBCS is located on human chromosome 6p22.3 and is modestly conserved among mammals (Supplementary Fig. S2B). In our assessment, the full-length *lnc-LBCS* transcript was 731 nt in the bladder cancer cell, which was examined using 5′ and 3′ rapid amplification of cDNA ends (RACE) and verified by Northern blotting (Supplementary Fig. S2C and S2D). In addition, *lnc-LBCS* displayed no protein coding potential (Supplementary Fig. S2E and S2F). Furthermore, cellular fractionation assays and RNA FISH showed that *lnc-LBCS* was mainly localized in the nuclei of bladder cancer cells (Supplementary Fig. S2G and S2H).

Lnc-LBCS associates with bladder cancer clinical characteristics and good prognosis

To investigate whether *lnc-LBCS* was involved in clinical bladder cancer progression, we detected and analyzed *lnc-LBCS* expression in three independent large-scale cohorts of bladder cancer specimens. Remarkably, *lnc-LBCS* was downregulated in bladder cancer tissues compared with normal tissues, and in high-grade compared with lower-grade tumors examined in a 120-case Cohort 1 (Fig. 1F and G). Moreover, statistical analysis revealed that *lnc-LBCS* expression was negatively correlated with pathologic grade and stage ($P = 0.002$ and 0.001, respectively, Supplementary Table S2). This result was further confirmed by analyses of a 185-case cohort in TCGA database and by ISH of an 86-case Cohort 2 (Fig. 1H–K; Supplementary Tables S3 and S4, and Supplementary Fig. S2I). Notably, *lnc-LBCS* displayed higher expression in neoadjuvant chemotherapy responders than nonresponders, suggesting that *lnc-LBCS* might be associated with chemoresistance (Fig. 1L). Furthermore, the Kaplan–Meier survival analysis showed that patients with low *lnc-LBCS*–expressing bladder cancers had significantly shorter OS and DFS in Cohort 1 and the TCGA Cohort (Fig. 1M–O). Multivariate analyses revealed that high *lnc-LBCS* expression was independent prognostic factor for OS and DFS in bladder cancer patients (Supplementary Tables S5 and S6). These data demonstrate that *lnc-LBCS* associates with cell differentiation of bladder cancer and may as a marker of good prognosis in bladder cancer.

Interestingly, further analyses of TCGA databases showed that *lnc-LBCS* expression was also significantly downregulated in other types of human cancer, such as lung, breast, stomach, and thyroid cancer, and head and neck squamous cell carcinoma (Supplementary Fig. S3A–S3F). High expression of *lnc-LBCS* correlated with good prognosis in many human cancers, such as lung cancer, head and neck squamous cell carcinoma, sarcoma, rectum adenocarcinoma, and uterine corpus endometrial carcinoma (Supplementary Fig. S3G–S3O), further supporting the tumor-suppressor role of *lnc-LBCS* in cancers.

Lnc-LBCS overexpression inhibits the self-renewal of BCSCs

To investigated the role of *lnc-LBCS* in BCSCs, we overexpressed *lnc-LBCS* in 5637 and BCSCs' UM-UC-3 4th cells, whereas silenced *lnc-LBCS* in 5637 and non-BCSCs' UM-UC-3 cells via lentivirus infection. The overexpression or knockdown efficiency was confirmed using qRT-PCR (Fig. 2A and B). *Lnc-LBCS* overexpression markedly decreased the number and size of spheres formation in UM-UC-3 4th and 5637 cells (Fig. 2C; Supplementary Fig. S4A). Serial sphere formation assays showed that *lnc-LBCS* overexpression inhibited long-term self-renewal over four generations of sphere formation (Supplementary Fig. S4B). Conversely, *lnc-LBCS* depletion significantly enhanced sphere formation in UM-UC-3 and 5637 cells (Fig. 2D; Supplementary Fig. S4C and S4D). Furthermore, flow cytometry analysis revealed that the population of $ALDH^+$ cells was significantly decreased by *lnc-LBCS* overexpression, whereas it was increased by *lnc-LBCS* depletion (Fig. 2E and F; Supplementary Fig. S4E and S4F). The *in vivo* tumor initiation assay showed that *lnc-LBCS*–transduced cells had remarkably weaker tumorigenic capacity and lower ratios of BCSCs than control cells (Fig. 2G–I; Supplementary Fig. S4G; Supplementary Fig. S5A–S5C and S5G), suggesting the repressive function of *lnc-LBCS* in tumor initiation. Besides, *lnc-LBCS*–transduced cells showed

Figure 1.

Lnc-LBCS is markedly downregulated in BCSCs and predicts good prognosis. **A,** Microarray analysis of BCSCs-associated lncRNAs in UM-UC-3 4th cells spheres, adhered for 10 or 1 day, and adherent UM-UC-3 cells. **B,** Three lncRNA expressions were analyzed by qRT-PCR in spheres adhered for 10 hours, 1, 3, 5 days, and adherent cells of UM-UC-3 4th. **C,** Expression of three lncRNAs in spheres and adherent cells derived from 5637, HT-1376, J82, and primary bladder cancer cells (Bca1) cells. **D,** Expression of three lncRNAs in ALDH-positive and -negative cells derived from UM-UC-3 and 5637 cells. **E,** Spheres formation assay of sh-OVAAL, sh-RP11-472G21, sh-*lnc-LBCS*, and sh-Ctrl UM-UC-3 and 5637 cells. Spheres were counted and compared on day 15. **F** and **G,** *Lnc-LBCS* expression was detected in bladder cancer tissues paired with NAT, and high-grade compared with lower-grade bladder cancer in Cohort 1. **H** and **I,** *Lnc-LBCS* expression was analyzed in TCGA cohort. **J** and **K,** Representative images of ISH of *lnc-LBCS* expression (blue) in paraffin-embedded NAT ($n = 20$), low-grade ($n = 25$), and high-grade ($n = 61$) bladder cancer. ISH of *lnc-LBCS* expression was quantified by the expression score (0–300). Red scale bars, 50 μm. **L,** *Lnc-LBCS* was detected in responders and nonresponders among patients with bladder cancer receiving neoadjuvant GC chemotherapy ($n = 24$). **M** and **N,** Kaplan–Meier curves for OS (**M**) and DFS (**N**) of bladder cancer patients with high vs. low expression of *lnc-LBCS* in Cohort 1. One hundred twenty patients with bladder cancer in Cohort 1 were divided into low *lnc-LBCS* ($n = 60$) and high *lnc-LBCS* groups ($n = 60$). **O,** Kaplan–Meier curves for OS of bladder cancer patients with high vs. low expression of *lnc-LBCS* in TCGA cohort. One hundred eighty-five patients with bladder cancer from the TCGA dataset were divided into low *lnc-LBCS* ($n = 115$) and high *lnc-LBCS* groups ($n = 70$). *, $P < 0.05$ and **, $P < 0.01$.

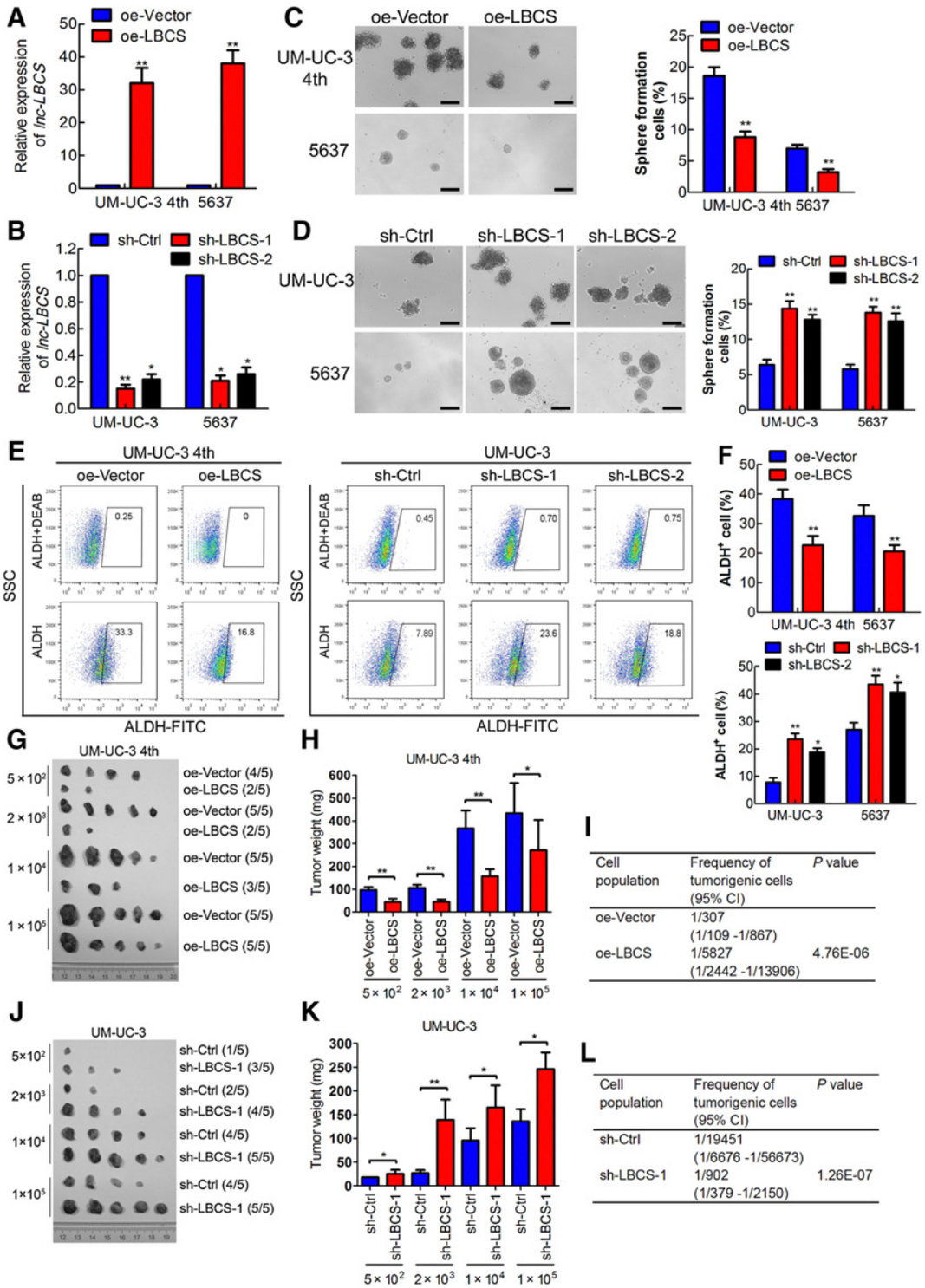

Figure 2.

Lnc-LBCS overexpression inhibits the self-renewal of BCSCs. **A** and **B,** qRT-PCR analysis of *lnc-LBCS* expression in *lnc-LBCS*–transduced, *lnc-LBCS*–silenced, and control cells as indicated. **C** and **D,** Representative images of spheres and histogram analysis of sphere-formation rates in the indicated cells. Black scale bars, 200 μm. **E** and **F,** Aldefluor analysis was performed to detect ALDH$^+$ cells in the indicated cells. **G–I,** *In vivo* tumor initiation assay of *lnc-LBCS*–transduced and control UM-UC-3 4th cells. **J–L,** *In vivo* tumor initiation assay of *lnc-LBCS*–silenced and control UM-UC-3 cells. Tumors were observed over 2 months; $n = 5$ for each group. Tumor pictures and tumor weight are shown. Tumorigenic cell frequency was analyzed using a limiting dilution assay. Data are shown as mean ± SD. *, $P < 0.05$ and **, $P < 0.01$.

reductive tumor propagation compared with control cells (Fig. 2G–I). In contrast, *lnc-LBCS* depletion contributed to much stronger tumor initiation and propagation, as well as higher tumorigenic cell frequency (Fig. 2J–L; Supplementary Fig. S4H; Supplementary Fig. S5D–S5F and S5H). To validate the results of *lnc-LBCS* knockdown, we also established *lnc-LBCS* KO cells using a CRISPR/Cas9 approach (Supplementary Fig. S6A and S6B). *Lnc-LBCS* KO cells displayed enhanced self-renewal capacity and tumor initiation of BCSCs *in vitro* and *in vivo* (Supplementary Fig. S6C–S6H), which agreed with the results of *lnc-LBCS* knockdown. Collectively, our results demonstrate that *lnc-LBCS* inhibits the self-renewal, tumor initiation, and propagation of BCSCs.

Lnc-LBCS suppresses chemoresistance of BCSCs *in vitro* and *in vivo*

Emerging evidence shows that CSCs are the main cause of chemotherapy resistance (5, 6). Gemcitabine and cisplatin are the first-line chemotherapeutic drug for bladder cancer. Therefore, we explored whether *lnc-LBCS* plays an important role in chemoresistance of BCSCs using the MTT assay, flow cytometry, and caspase-3/7 activity. Interestingly, *lnc-LBCS* overexpression markedly reduced chemotherapy resistance and the IC_{50} value, and increased the apoptosis rate and caspase-3/7 activity in UM-UC-3 4th and 5637 cells treated with gemcitabine or cisplatin, whereas the opposite outcome was observed after *lnc-LBCS* depletion (Fig. 3A–D; Supplementary Fig. S7A–S7C). Similar observations were obtained in the *lnc-LBCS* KO cells (Supplementary Fig. S9A–S9D). The ability of *lnc-LBCS* to regulate chemoresistance in BCSCs was further examined using an *in vivo* tumor model. Interestingly, after treated with GC chemotherapy, the relative tumor growth, the size, and weight in the *lnc-LBCS* overexpression group were significantly decreased compared with the control group (Fig. 3E–G; Supplementary Fig. S8A–S8C). Moreover, the tumors derived from the *lnc-LBCS* overexpression group exhibited a higher proportion of TUNEL-positive cells and lower Ki67 expression compared with the control group when treated with GC chemotherapy (Fig. 3H; Supplementary Fig. S7D and S7E; Supplementary Fig. S8G and S8I). Conversely, *lnc-LBCS* depletion significantly enhanced tumor growth and reduced apoptosis when treated with GC chemotherapy (Fig. 3I–L; Supplementary Fig. S7D and S7E; Supplementary Fig. S8D–S8F, S8H, and S8I). Consistent with the *lnc-LBCS* knockdown findings above, *lnc-LBCS* KO promoted the chemoresistance of BCSCs *in vivo* (Supplementary Fig. S9E–S9J). Overall, these data strongly indicate that *lnc-LBCS* suppresses chemoresistance of BCSCs *in vitro* and *in vivo*.

Lnc-LBCS directly binds to hnRNPK and EZH2, and serves as a scaffold to induce the formation of hnRNPK–EZH2 complex

To further identify the molecular mechanism and binding partners of *lnc-LBCS* in BCSCs, we performed RNA pulldown with biotin-labeled *lnc-LBCS*. Two overtly differential bands appeared by silver staining and were identified as hnRNPK and EZH2 by mass spectrometry (Fig. 4A; Supplementary Fig. S10A and S10B). We confirmed the special interaction of *lnc-LBCS*, hnRNPK, and EZH2 using Western blotting (Fig. 4B). We also verified this result using RIP assay and found that *lnc-LBCS* were enriched in both hnRNPK and EZH2 precipitates (Fig. 4C). We next constructed a series of *lnc-LBCS* truncations to map its binding fragment with the hnRNPK and EZH2. We found that the 240–480 nt fragment of *lnc-LBCS* was sufficient to bind hnRNPK (Fig. 4D). Considering that hnRNPK binds to pyrimidine-rich sequences (32, 33), we identified the accurate binding site of hnRNPK in *lnc-LBCS* (256–280 nt) via RNA pulldown assays (Fig. 4E). The 240–731 nt fragment of *lnc-LBCS* was sufficient to bind EZH2, but not 1–480 nt or 480–731 nt, suggesting that the binding site was around 480 nt (Fig. 4D). Considering that EZH2 binds to stem-loop structure of RNA (34), we deduced that EZH2 bound to the 468–523 nt fragment of *lnc-LBCS* which formed a stem-loop structure (Fig. 4F).

To determine whether hnRNPK and EZH2 interact with *lnc-LBCS* independently or as a multiprotein complex, we performed co-IP assay followed by Western blotting (Fig. 4G). Interestingly, hnRNPK and EZH2 interactions were observed significantly in lysates incubated with the *lnc-LBCS* RNA, but not the mock group. However, these interactions were abolished by treatment of lysates with ribonuclease (RNase; Fig. 4G), suggesting that *lnc-LBCS* RNA was essential to the formation of hnRNPK–EZH2 complex. Taken together, these results indicate that *lnc-LBCS* directly binds to hnRNPK and EZH2, and serves as a scaffold to induce the formation of this complex.

Lnc-LBCS regulates SOX2 expression by forming triplexes with the promoter sequences of SOX2

To explore the target genes of *lnc-LBCS* in BCSCs, we investigated self-renewal and chemoresistance pathway genes in *lnc-LBCS*–silenced cells. Interestingly, SOX2 was the most significant upregulated gene in *lnc-LBCS*–silenced cells (Fig. 5A). Furthermore, the mRNA and protein levels of SOX2 were increased in *lnc-LBCS*–silenced and *lnc-LBCS*-KO cells, whereas they were decreased in *lnc-LBCS*–overexpressing cells (Fig. 5B and C; Supplementary Fig. S11A). To further verify the correlation between *lnc-LBCS* and SOX2, we detected the expression of SOX2 in two independent cohorts of bladder cancer specimens by qRT-PCR and IHC. Notably, the mRNA and the protein levels of SOX2 correlated negatively with the *lnc-LBCS* level (Fig. 5D–F, $P < 0.001$, $P < 0.001$, respectively). In summary, these data indicated that *lnc-LBCS* inhibited SOX2 expression.

To provide direct evidence that *lnc-LBCS* associated with the promoter region of SOX2, we performed ChIRP experiment and detected the enrichment of specific regulatory regions by qPCR. We observed obvious enrichment of the −810 to −927 nt region of the SOX2 promoter using *lnc-LBCS* probes, but no enrichment of GAPDH or other regions of the SOX2 promoter, as compared with LacZ probes. TERC and its downstream gene WNT-1 served as positive controls for RNA and DNA enrichment (Fig. 5G and H; Supplementary Fig. S11B–S11E). To further identify more precisely the direct binding sites between *lnc-LBCS* and the SOX2 promoter, we analyzed potential triplex-forming oligos (TFO) and corresponding triplex target sites (TTS) using the Longtarget software (35). Fluorescence resonance energy transfer (FRET) was performed using *in vitro* synthesized predicted TFOs of *lnc-LBCS* and TTSs of the SOX2 promoter. Upon excitation at 460 nm, the emission at 580 nm increased, whereas the signal at 520 nm decreased in the *lnc-LBCS* (246–266 nt)/SOX2

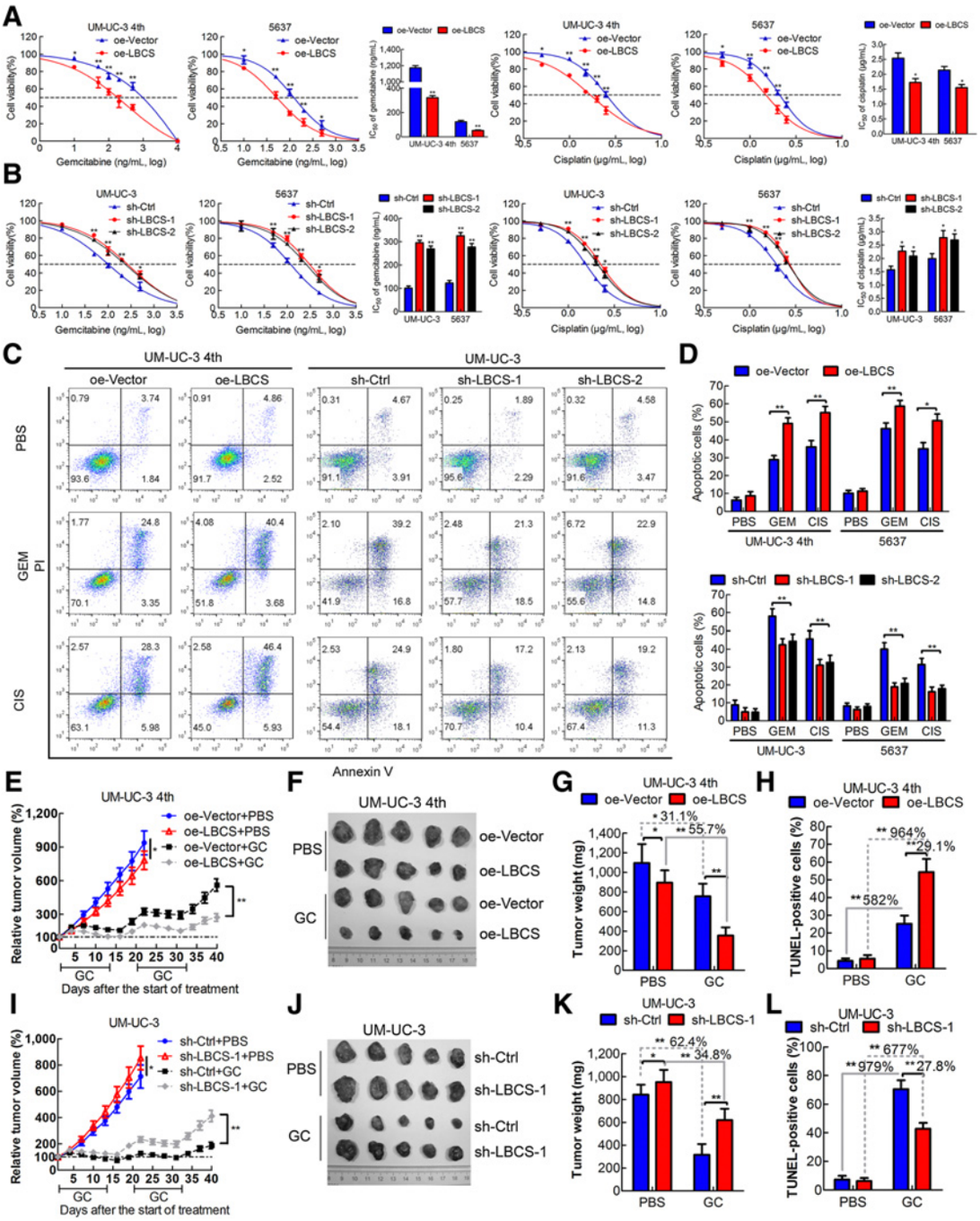

Figure 3.

Lnc-LBCS suppresses chemoresistance of BCSCs *in vitro* and *in vivo*. **A** and **B,** *Lnc-LBCS* overexpression, *lnc-LBCS* knockdown, and corresponding control cells were treated with increasing concentrations of gemcitabine or cisplatin for 48 hours. Cellular viability was determined by MTT assay, and the IC_{50} values were calculated based on a nonlinear regression analysis. **C** and **D,** The apoptosis analysis of *lnc-LBCS* overexpression, *lnc-LBCS* knockdown, and corresponding control cells treated with gemcitabine (400 ng/mL) or cisplatin (2 μg/mL) for 36 hours. The histogram shows the percentage (%) of apoptotic cells. **E** and **F,** The tumor growth of *lnc-LBCS* overexpression and control UM-UC-3 4th cells grafted mice treated with PBS or GC chemotherapy was measured every 3 days. The relative tumor volume was normalized to each group on day 0 of treatment, and relative tumor growth curve was calculated. Representative images of tumors of each group ($n = 5$). **G,** The weight of tumors was measured after the tumors were surgically dissected. **H,** The apoptosis in the tumor was detected by TUNEL assay. The histograms showed the proportion of TUNEL-positive cells in each group. The percentage in the histograms indicates the decreased or increased percentage in the GC group compared with the PBS group. **I–L,** The relative tumor growth curve (**I**), representative images of tumors (**J**), the weight of tumors (**K**), and the proportion of TUNEL-positive cells (**L**) of *lnc-LBCS*–silenced and control UM-UC-3 cells were shown as indicated. Data are shown as mean ± SD. *, $P < 0.05$ and **, $P < 0.01$.

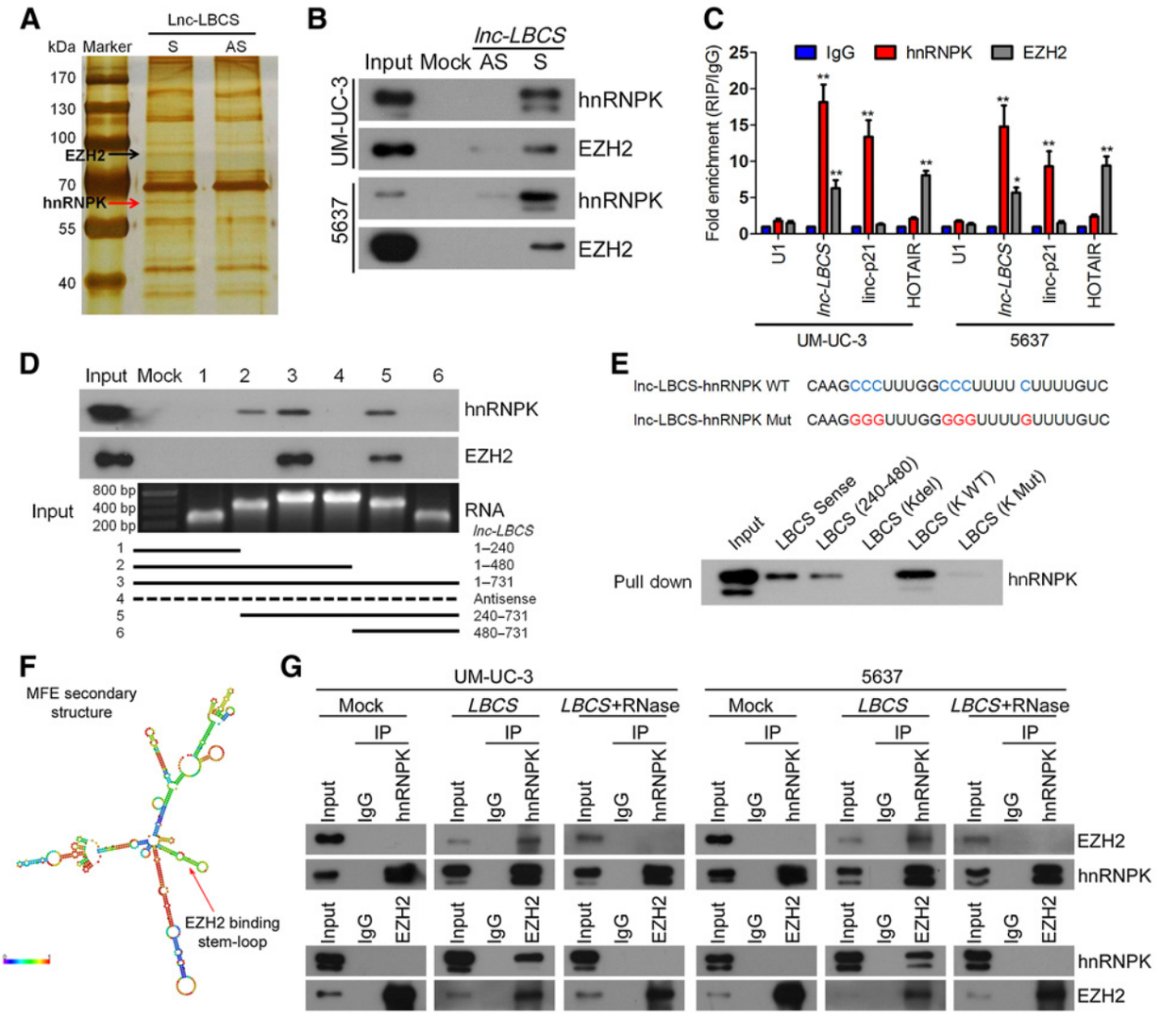

Figure 4.

Lnc-LBCS directly binds to hnRNPK and EZH2, and serves as a scaffold to induce the formation of this complex. **A,** RNA pulldown assay was performed using *lnc-LBCS* sense and antisense RNAs incubated with nuclear extracts of UM-UC-3 cells, followed by silver staining. A red arrow indicates hnRNPK, and a black arrow indicates EZH2. **B,** The interaction among *lnc-LBCS*, hnRNPK, and EZH2 was confirmed by RNA pulldown and Western blotting. **C,** RIP was performed using anti-hnRNPK, anti-EZH2, and control IgG antibodies, followed by qRT-PCR to examine the enrichment of *lnc-LBCS*, lincRNA-p21 (linc-p21), HOTAIR, and U1. LincRNA-p21 and HOTAIR served as positive controls, whereas U1 served as negative controls, respectively. **D,** Serial deletions of *lnc-LBCS* were used in the RNA pulldown assays to identify the core regions of *lnc-LBCS* that were required for the physical interaction with hnRNPK and EZH2. **E,** RNA pulldown assay was performed to validate the hnRNPK-binding site by using biotin-labeled *lnc-LBCS* sense, 240–480 nt, *lnc-LBCS* with hnRNPK-binding site deletion (K Del), hnRNPK-binding site wild-type and mutated RNA, followed by Western blotting. **F,** Prediction of *lnc-LBCS* structure was based on minimum free energy (MFE) and partition function (http://rna.tbi.univie.ac.at/). A red arrow indicates the EZH2-binding stem-loop structure. **G,** Co-IP assay was performed to verify that *lnc-LBCS* induced formation of hnRNPK and EZH2 complex. Nuclear extracts of cell were incubated with the indicated antibody and RNA. Mock, *LBCS*, and *LBCS*+RNase indicated no RNA, *in vitro* transcription *lnc-LBCS* RNA, and *lnc-LBCS* RNA mixed with Ribonuclease (RNase), respectively. Data are shown as mean ± SD. *, $P < 0.05$ and **, $P < 0.01$.

TTS group compared with that of the control RNA/SOX2 TTS (Fig. 5I). However, *lnc-LBCS* (mut)/SOX2 TTS and *lnc-LBCS* (246–266 nt)/SOX2 TTS (mut) did not influence the signals at 520 and 580 nm (Fig. 5I; Supplementary Fig. S11G). Taken together, these data indicate that *lnc-LBCS* 246–266 nt fragment directly forms triplexes with the promoter sequences of SOX2.

Lnc-LBCS guides hnRNPK–EZH2 complex to the SOX2 promoter and induces H3K27me3

Through analysis of the histone modification profile in the UCSC genome browser, we found that the *lnc-LBCS*–binding region in the SOX2 promoter had a high H3K27me3 level, suggesting that *lnc-LBCS* might recruit hnRNPK–EZH2 complex to mediate H3K27me3 on SOX2 promoter (Supplementary

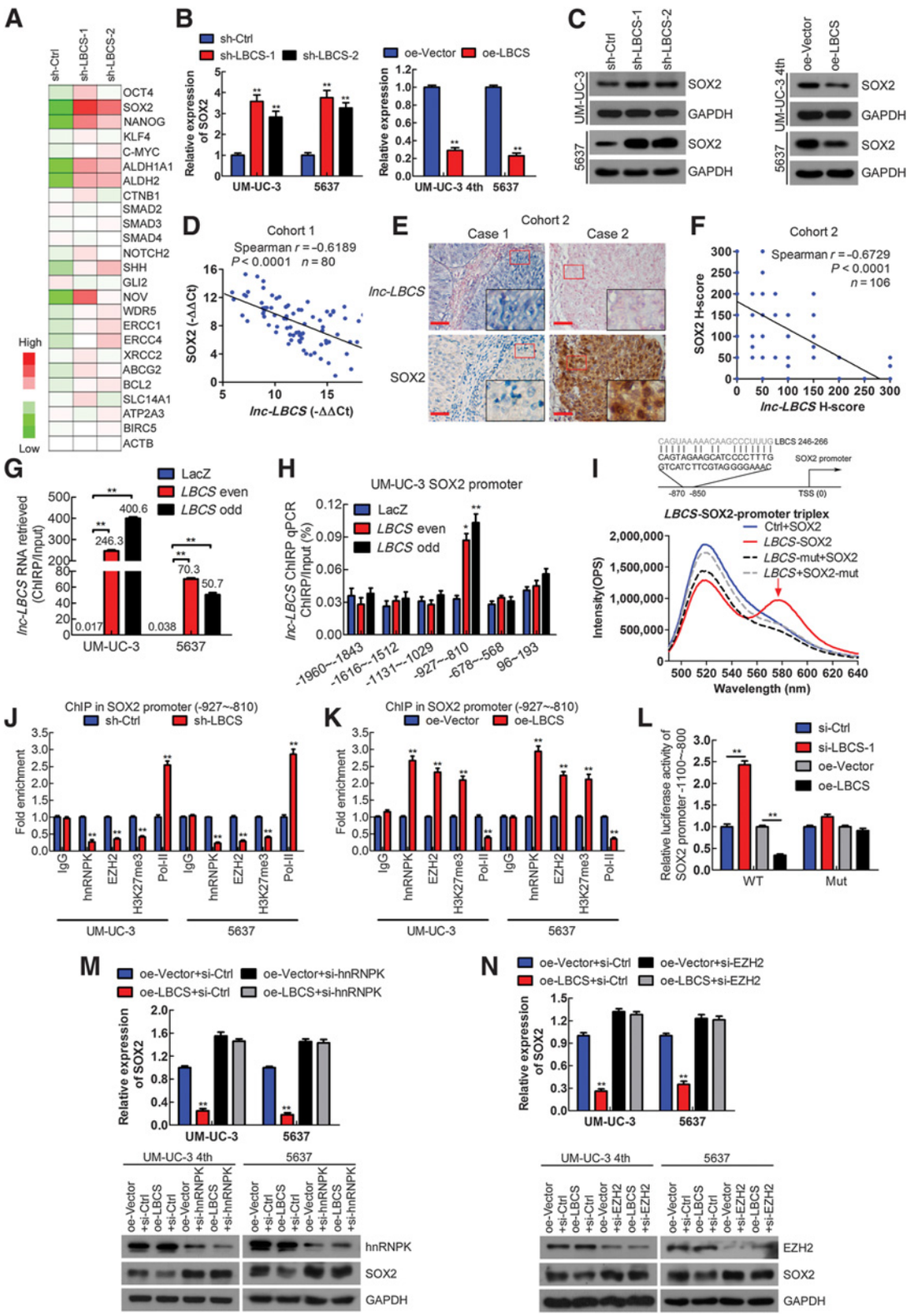

Fig. S11F). To address this, we performed a ChIP assay and qPCR. *Lnc-LBCS* knockdown resulted in decreased location of hnRNPK, EZH2, and H3K27me3 but increased location of RNA polymerase-II on the promoter regions of SOX2, but not on the negative control (Fig. 5J; Supplementary Fig. S11H). Furthermore, we found that *lnc-LBCS* knockdown enhanced the luciferase activity in the wild-type–binding region of SOX2, but not in the mutated region (Fig. 5L). Conversely, *lnc-LBCS* overexpression augmented the location of hnRNPK, EZH2, and H3K27me3, but reduced RNA polymerase-II binding to the SOX2 promoter (Fig. 5K; Supplementary Fig. S11H). Similarly, *lnc-LBCS* overexpression attenuated the luciferase activity, but not when including the mutated region (Fig. 5L). Furthermore, knockdown of hnRNPK or EZH2 rescued the depression effect of *lnc-LBCS* on chemoresistance and SOX2 in bladder cancer cells (Fig. 5M and N; Supplementary Fig. S12). Overall, these data indicate that *lnc-LBCS* inhibits SOX2 transcription by directly guiding hnRNPK–EZH2 complex to mediate H3K27me3 of the SOX2 promoter.

SOX2 is required for self-renewal and chemoresistance of BCSCs and rescues the suppressive effect of *lnc-LBCS*

Accumulating evidence shows that SOX2 plays a key role in tumor initiation and self-renewal of CSCs in several cancers (36); however, its effect on self-renewal and chemoresistance of BCSCs remains unclear. We stably upregulated SOX2 in control vector and *lnc-LBCS*–overexpressing cells, which was verified by qRT-PCR and Western blotting (Supplementary Fig. S13A and S13B). SOX2 upregulation significantly promoted BCSCs' sphere formation and increased the population of $ALDH^+$ cells *in vitro*, and enhanced tumor initiation *in vivo*. Moreover, SOX2 overexpression also rescued the inhibitory effects of *lnc-LBCS* on the self-renewal of BCSCs *in vitro* and *in vivo* (Fig. 6A–D; Supplementary Fig. S13C–S13E). Notably, SOX2 overexpression markedly enhanced the chemoresistance of BCSCs to gemcitabine and cisplatin *in vitro* and *in vivo*. In addition, SOX2 overexpression also rescued the repressive roles of *lnc-LBCS* on the chemoresistance of BCSCs (Fig. 6E–I; Supplementary Fig. S14A–S14G). In summary, these findings indicate that SOX2 is required for self-renewal and chemoresistance of BCSCs and rescues the suppressive effect of *lnc-LBCS*.

To further verify the roles of *lnc-LBCS* in BCSCs in an SOX2-dependent manner, we overexpressed *lnc-LBCS* and truncated *lnc-LBCS* without the SOX2 promoter binding site (*lnc-LBCS* Sdel) in UM-UC-3 4th and 5637 cells, respectively. Interestingly, the *lnc-LBCS* Sdel group did not inhibit sphere formation or reduce the population of $ALDH^+$ cells compared with the control vector group (Supplementary Fig. S15A–S15C). Similarly, compared with the control vector group, overexpression of *lnc-LBCS* Sdel did not affect the chemotherapy resistance, IC_{50} value, apoptosis rate, and caspase-3/7 activity in UM-UC-3 4th and 5637 cells treated with gemcitabine or cisplatin (Supplementary Fig. S15D–S15H). Overall, the SOX2-binding site of *lnc-LBCS* is essential for *lnc-LBCS* to exert the inhibitory effect on SOX2 expression and BCSCs' functions.

Expression levels of SOX2 are positively correlated with severity and prognosis of bladder cancer patients

Finally, we investigated the clinical significance of SOX2 expression in bladder cancer tumorigenesis and progression in three independent large-scale cohorts. Interestingly, high expression levels of SOX2 were found in bladder cancer samples and high-grade samples, indicating the potential role of SOX2 in bladder cancer initiation and stemness (Fig. 6J and K). Moreover, clinical correlation analysis revealed that SOX2 expression was strongly correlated with pathologic grade and stage ($P = 0.001$ and $P < 0.001$, respectively; Supplementary Table S7). This finding was further confirmed by IHC of an 86-case Cohort 2 and TCGA cohort bladder cancer samples (Fig. 6L and M; Supplementary Table S8; Supplementary Fig. S16A). Notably, SOX2 displayed higher expression in neoadjuvant chemotherapy nonresponders than responders, further conforming that SOX2 was associated with chemoresistance (Supplementary Fig. S16B). Furthermore, the Kaplan–Meier survival analysis found that patients with high SOX2 expression had shorter OS and DFS in Cohort 1 and in the TCGA cohort (Fig. 6N–Q). Besides its role in stemness maintenance and development regulation, we revealed the critical role of SOX2 in bladder cancer initiation, progress, and prognosis prediction.

Collectively, the absence of *lnc-LBCS* in BCSCs attenuates the recruitment and location of hnRNPK–EZH2 complex on the SOX2 promoter, which increases SOX2 expression, contributing to the survival advantage in response to chemotherapy and subsequent tumor relapse. In non-BCSCs, *lnc-LBCS* could guide the hnRNPK–EZH2 complex to suppress SOX2 expression, leading to good response to chemotherapy (Fig. 6R).

Discussion

LncRNAs are reported to have important epigenetic regulatory roles in diverse biological cellular processes including

Figure 5.

Lnc-LBCS guides hnRNPK–EZH2 complex to inhibit SOX2 expression via inducing H3K27me3. **A,** qRT-PCR analysis of self-renewal and chemoresistance pathway genes in *lnc-LBCS*–silenced cells, shown as heat map. **B** and **C,** qRT-PCR and Western blotting detection of SOX2 mRNA and protein levels in *lnc-LBCS*–silenced and –overexpressing bladder cancer cells. **D,** qRT-PCR analysis of the correlation between the transcription level of *lnc-LBCS* and SOX2 in 80 bladder cancer samples. Data were normalized to GAPDH and analyzed by Spearman correlation analysis. **E** and **F,** Representative images (**E**) and Spearman correlation analyses (**F**) of IHC staining showing that *lnc-LBCS* expression negatively correlates with SOX2 ($n = 106$). Scale bars, 50 μm. **G** and **H,** ChIRP analysis of *lnc-LBCS*–associated chromatin in UM-UC-3 and 5637 cells. Retrieved *lnc-LBCS* RNA (**G**) was quantified qRT-PCR. Retrieved chromatin (**H**) was quantified by qPCR. Values were normalized to the input and presented as the mean ± SD. **I,** A putative SOX2-binding site was identified in *lnc-LBCS* (top plot). FRET was performed using a 5:1 mixture of TFO with TTSs in the SOX2 promoter sequences (bottom plot). **J** and **K,** ChIP-qPCR analysis of the hnRNPK, EZH2, and RNA polymerase II (Pol-II) genomic occupancy and H3K27 methylation status in the SOX2 promoter after depletion (**J**) or overexpression (**K**) of *lnc-LBCS* in UM-UC-3 and 5637 cells. Values are normalized to the sh-control or oe-vector groups. **L,** SOX2 (–1,100 to –800) wild-type or *lnc-LBCS*–binding site-mutated promoters were constructed in the pGL3 vector and subjected to luciferase reporter assays in *lnc-LBCS*– silenced and overexpression cells. **M** and **N,** qRT-PCR and Western blotting detection of SOX2 mRNA and protein levels in *lnc-LBCS*–overexpressing or control cells combined with knockdown of hnRNPK or EZH2, respectively. Data are shown as mean ± SD. *, $P < 0.05$ and **, $P < 0.01$.

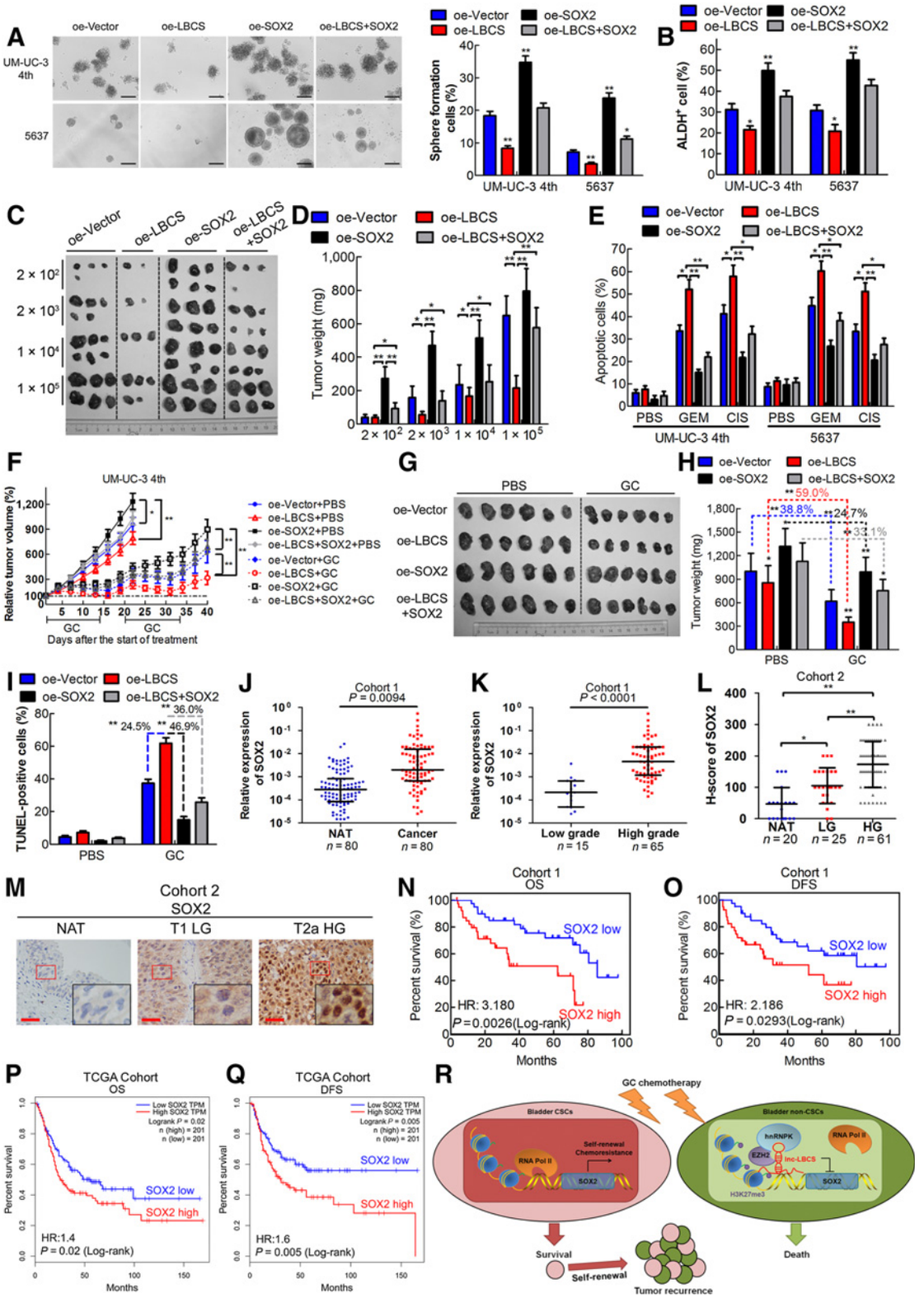

tumorigenesis and cancer chemoresistance. In this study, we first reported that a novel lncRNA-*LBCS* is significantly downregulated in BCSCs and cancer tissue, and correlates with tumor grade, chemotherapy response, and prognosis. Moreover, *lnc-LBCS* markedly suppressed the self-renewal and chemoresistance of BCSCs by guiding the hnRNPK–EZH2 complex to inhibit SOX2 expression, thereby contributing to attenuate bladder cancer initiation and chemoresistance. These findings indicate that *lnc-LBCS* acts as a tumor suppressor in bladder tumorigenesis and progression, and could be considered as a potential prognostic indicator and therapy target for bladder cancer.

Recent studies show that lncRNAs, including lncTCF7 (16), lncARSR (17), RBM5-AS1 (18), and ICR (37), participate in CSCs' self-renewal of liver, renal, and colon cancer. However, the BCSCs-associated lncRNAs remain largely unknown. Here, through transcriptome microarray analysis and verification in several BCSCs models, we identified a novel lncRNA-*LBCS* that was significantly downregulated in BCSCs, and its expression gradually increased during spheres readherence. Importantly, *lnc-LBCS* expression was negatively correlated with bladder cancer grade and stage in three independent cohorts, whereas it was positively correlated with neoadjuvant chemotherapy response and good prognosis, suggesting that *lnc-LBCS* could regulate cell differentiation and chemosensitivity. Furthermore, analyses of TCGA databases showed that *lnc-LBCS* was also downregulated and correlated with prognosis in various types of human cancers, suggesting a common tumor-suppressor role of *lnc-LBCS*.

LncRNAs can guide and recruit histone protein modification enzymes or transcription factors to specific genomic loci, leading to inactivation or activation of genes (38). HnRNPK is an essential RNA- and DNA-binding protein that plays a critical role in several cancers (24, 39). Our previous study found that hnRNPK regulates diverse functions in bladder cancer by directly mediating transcription of target genes; however, the detailed mechanism remained unclear (24). EZH2, a histone methyl transferase subunit of the polycomb repressor complex 2 (PRC2), is an oncogene that is central to tumor proliferation, metastasis, and self-renewal (40, 41). In the present study, we found that *lnc-LBCS* physically interacts with hnRNPK and EZH2, and *lnc-LBCS* serves as a scaffold to induce the formation of hnRNPK–EZH2 complex. Furthermore, *lnc-LBCS* recruited this complex to the SOX2 promoter and suppressed SOX2 expression via mediating H3K27me3. Although hnRNPK and EZH2 are overexpressed and exert oncogenic function in several cancers, recent study indicates that some lncRNAs could recruit hnRNPK or EZH2 to exert a tumor-suppressor role. For example, lincRNA-p21 recruits hnRNPK to inhibit p53-pathway genes (42), and MEG3 recruits EZH2 to inhibit metastasis of breast cancer cells by repressing TGFβ pathway genes (43). These findings suggested that recruitment and guidance by lncRNAs might decide target gene regulation and the function of hnRNPK and EZH2 in cancer. The low expression of *lnc-LBCS* in BCSCs would result in attenuated recruitment and location of hnRNPK–EZH2 complex on the SOX2 promoter, contributing to SOX2 upregulation in BCSCs and bladder cancer progression.

SOX2 is a master regulator that maintains stemness in embryonic stem cells (44) as well as self-renewal of CSCs in several malignancies (36, 45). In addition, SOX2 also plays a critical role in drug resistance to paclitaxel (45) and gemcitabine (46) in several cancers. However, the function and epigenetic regulatory mechanism of SOX2 in BCSCs remain to be determined. In this study, we demonstrated that SOX2 is required for the self-renewal and chemoresistance to gemcitabine and cisplatin of BCSCs and tumor propagation by acting as a key oncogene. Intriguingly, a previous study revealed that the expression of SOX2 during the course of carcinogenesis correlates with a loss of the repressive H3K27me3 chromatin mark at the SOX2 promoter (36), but the underlying mechanism was unclear. Here, we found that SOX2 is markedly repressed by *lnc-LBCS*, which recruits hnRNPK–EZH2 complex to SOX2 promoter leading to H3K27me3. While we were submitting this article, we noted a similar finding by Ooki and colleagues recently reported that YAP1 and COX2 coordinately enhanced SOX2 to promote chemoresistance of BCSCs (47). Similarly, Zhu and colleagues reported that SOX2 is a marker for stem-like tumor cells in bladder cancer (48). Consistent with our finding, these two studies indicate that SOX2 plays a major role in BCSCs. Collectively, our finding reveals a novel epigenetic regulation mechanism of SOX2 by *lnc-LBCS* in BCSCs, suggesting that *lnc-LBCS* may represent a new target for intervention in SOX2-dependent BCSCs.

In conclusion, it is our novel discovery that *lnc-LBCS* can inhibit BCSCs' self-renewal and chemoresistance by repression of SOX2 via guiding hnRNPK–EZH2 complex to the SOX2 promoter and inducing H3K27me3. Therefore, our findings provide insight into *lnc-LBCS* might be used in diagnosis and prognosis for bladder cancer, as well as in the development of novel therapeutic drugs against chemoresistant BCSCs.

Disclosure of Potential Conflicts of Interest

No potential conflicts of interest were disclosed.

Figure 6.

SOX2 is required for self-renewal and chemoresistance of BCSCs and positively correlated with poor prognosis. **A** and **B,** The spheres formation (**A**) and Aldefluor analysis (**B**) were performed to investigate the effects of SOX2 on self-renewal in control vector and *lnc-LBCS*–overexpressing bladder cancer cells *in vitro*. Black scale bars, 200 μm. **C** and **D,** The tumor initiation assay was performed to investigate the effects of SOX2 on self-renewal *in vivo*. **E–I,** apoptotic flow cytometry (**E**), *in vivo* tumor chemotherapy (**F–H**), and TUNEL (**I**) assays were used to study the effect of SOX2 on chemoresistance *in vitro* and *in vivo*. Six mice were used in each group. **J** and **K,** SOX2 expression was detected in bladder cancer tissues paired with NAT, and high-grade compared with lower-grade bladder cancer in Cohort 1. **L** and **M,** Representative images of the IHC of SOX2 expression in the paraffin-embedded NAT ($n = 20$), low-grade ($n = 25$), and high-grade ($n = 61$) bladder cancer in Cohort 2. IHC of SOX2 expression was quantified by the expression score (0–300). Red scale bars, 50 μm. **N** and **O,** Kaplan–Meier curves for OS (**N**) and DFS (**O**) of bladder cancer patients with high vs. low expression of SOX2 in Cohort 1. **P** and **Q,** Kaplan–Meier curves for OS (**P**) and DFS (**Q**) of bladder cancer patients with high vs. low expression of SOX2 in TCGA cohort. The median was chosen as the cutoff point in Cohort 1 and TCGA cohort. **R,** A schematic model of the mechanism underlying the role of *lnc-LBCS* in BCSCs' self-renewal and chemoresistance. *, $P < 0.05$ and **, $P < 0.01$.

Authors' Contributions

Conception and design: X. Chen, J. Huang, T. Lin
Development of methodology: X. Chen, P. Gu, B. Wang, G. Zhong, Z. Chen
Acquisition of data (provided animals, acquired and managed patients, provided facilities, etc.): X. Chen, R. Xie, P. Gu, M. Huang, W. Dong, W. Xie
Analysis and interpretation of data (e.g., statistical analysis, biostatistics, computational analysis): J. Han, W. Dong, G. Zhong
Writing, review, and/or revision of the manuscript: X. Chen, J. Huang, T. Lin
Study supervision: W. He, J. Huang, T. Lin

Acknowledgments

This study was supported by the National Natural Science Foundation of China (grant nos. 81825016, 81702523, 81772719, 81772728, 81572514, and 81472384), National Natural Science Foundation of Guangdong (grant nos. 2016A030313321, 2016A030313244, and 2015A030311011), Science and Technology Program of Guangzhou (grant nos. 201804010041, 201604020156, and 201604020177), the Science and Technology Planning Project of Guangdong Province (grant no. 2017B020227007), Guangdong Special Support Program (2017TX04R246), the Fundamental Research Funds for the Central Universities (for X. Chen, 18ykpy18), Project Supported by Guangdong Province Higher Vocational Colleges & Schools Pearl River Scholar Funded Scheme (for T. Lin), Yat-Sen Scholarship for Young Scientist (for X. Chen), Sun Yat-sen Initiative Program for Scientific Research (for X. Chen, YXQH201708), Cultivation of Major Projects and Emerging, Interdisciplinary Fund, Sun Yat-Sen University (grant no. 16ykjc18), and National Clinical Key Specialty Construction Project for Department of Urology and Department of Oncology. This study was also supported by grant KLB09001 from the Key Laboratory of Malignant Tumor Gene Regulation and Target Therapy of Guangdong Higher Education Institutes, Sun-Yat-Sen University, and grant [2013]163 from Key Laboratory of Malignant Tumor Molecular Mechanism and Translational Medicine of Guangzhou Bureau of Science and Information Technology.

The costs of publication of this article were defrayed in part by the payment of page charges. This article must therefore be hereby marked *advertisement* in accordance with 18 U.S.C. Section 1734 solely to indicate this fact.

Received May 28, 2018; revised September 18, 2018; accepted November 2, 2018; published first November 5, 2018.

References

1. Torre LA, Bray F, Siegel RL, Ferlay J, Lortet-Tieulent J, Jemal A. Global cancer statistics, 2012. CA Cancer J Clin 2015;65:87–108.
2. Gerlinger M, Catto JW, Orntoft TF, Real FX, Zwarthoff EC, Swanton C. Intratumour heterogeneity in urologic cancers: from molecular evidence to clinical implications. Eur Urol 2015;67:729–37.
3. Clevers H.The cancer stem cell: premises, promises and challenges. Nat Med 2011;17:313–9.
4. Kurtova AV, Xiao J, Mo Q, Pazhanisamy S, Krasnow R, Lerner SP, et al. Blocking PGE2-induced tumour repopulation abrogates bladder cancer chemoresistance. Nature 2015;517:209–13.
5. Vidal SJ, Rodriguez-Bravo V, Galsky M, Cordon-Cardo C, Domingo-Domenech J. Targeting cancer stem cells to suppress acquired chemotherapy resistance. Oncogene 2014;33:4451–63.
6. Beck B, Blanpain C. Unravelling cancer stem cell potential. Nat Rev Cancer 2013;13:727–38.
7. Chan KS, Espinosa I, Chao M, Wong D, Ailles L, Diehn M, et al. Identification, molecular characterization, clinical prognosis, and therapeutic targeting of human bladder tumor-initiating cells. PNAS 2009;106:14016–21.
8. Ho PL, Kurtova A, Chan KS. Normal and neoplastic urothelial stem cells: getting to the root of the problem. Nat Rev Urol 2012;9:583–94.
9. Su Y, Qiu Q, Zhang X, Jiang Z, Leng Q, Liu Z, et al. Aldehyde dehydrogenase 1 A1-positive cell population is enriched in tumor-initiating cells and associated with progression of bladder cancer. Cancer Epidemiol Biomark Prev 2010;19:327–37.
10. Ferreira-Teixeira M, Parada B, Rodrigues-Santos P, Alves V, Ramalho JS, Caramelo F, et al. Functional and molecular characterization of cancer stem-like cells in bladder cancer: a potential signature for muscle-invasive tumors. Oncotarget 2015;6:36185–201.
11. Batista PJ, Chang HY. Long noncoding RNAs: cellular address codes in development and disease. Cell 2013;152:1298–307.
12. Perry RB, Ulitsky I. The functions of long noncoding RNAs in development and stem cells. Development 2016;143:3882–94.
13. Schmitt AM, Chang HY. Long noncoding RNAs in cancer pathways. Cancer Cell 2016;29:452–63.
14. Liu B, Sun L, Liu Q, Gong C, Yao Y, Lv X, et al. A cytoplasmic NF-kappaB interacting long noncoding RNA blocks IkappaB phosphorylation and suppresses breast cancer metastasis. Cancer Cell 2015;27:370–81.
15. Yue B, Cai D, Liu C, Fang C, Yan D. Linc00152 functions as a competing endogenous RNA to confer oxaliplatin resistance and holds prognostic values in colon cancer. Mol Ther 2016;24:2064–77.
16. Wang Y, He L, Du Y, Zhu P, Huang G, Luo J, et al. The long noncoding RNA lncTCF7 promotes self-renewal of human liver cancer stem cells through activation of Wnt signaling. Cell Stem Cell 2015;16:413–25.
17. Qu L, Wu Z, Li Y, Xu Z, Liu B, Liu F, et al. A feed-forward loop between lncARSR and YAP activity promotes expansion of renal tumour-initiating cells. Nat Commun 2016;7:12692.
18. Di Cecilia S, Zhang F, Sancho A, Li S, Aguilo F, Sun Y, et al. RBM5-AS1 is critical for self-renewal of colon cancer stem-like cells. Cancer Res 2016;76:5615–27.
19. Robertson AG, Kim J, Al-Ahmadie H, Bellmunt J, Guo G, Cherniack AD, et al. Comprehensive molecular characterization of muscle-invasive bladder cancer. Cell 2017;171:540–56 e25.
20. Li J, Han L, Roebuck P, Diao L, Liu L, Yuan Y, et al. TANRIC: an interactive open platform to explore the function of lncRNAs in Cancer. Cancer Res 2015;75:3728–37.
21. Tang Z, Li C, Kang B, Gao G, Li C, Zhang Z. GEPIA: a web server for cancer and normal gene expression profiling and interactive analyses. Nucleic Acids Res 2017;45:W98–W102.
22. Fan X, Chen X, Deng W, Zhong G, Cai Q, Lin T. Up-regulated microRNA-143 in cancer stem cells differentiation promotes prostate cancer cells metastasis by modulating FNDC3B expression. BMC Cancer 2013;13:61.
23. Chen X, Xie W, Gu P, Cai Q, Wang B, Xie Y, et al. Upregulated WDR5 promotes proliferation, self-renewal and chemoresistance in bladder cancer via mediating H3K4 trimethylation. Sci Rep 2015;5:8293.
24. Chen X, Gu P, Xie R, Han J, Liu H, Wang B, et al. Heterogeneous nuclear ribonucleoprotein K is associated with poor prognosis and regulates proliferation and apoptosis in bladder cancer. J Cell Mol Med 2017;21:1266–79.
25. Gu P, Chen X, Xie R, Han J, Xie W, Wang B, et al. lncRNA HOXD-AS1 regulates proliferation and chemo-resistance of castration-resistant prostate cancer via recruiting WDR5. Mol Ther 2017;25:1959–73.
26. He W, Zhong G, Jiang N, Wang B, Fan X, Chen C, et al. Long noncoding RNA BLACAT2 promotes bladder cancer-associated lymphangiogenesis and lymphatic metastasis. J Clin Invest 2018;128:861–75.
27. Jiang J, Chen X, Liu H, Shao J, Xie R, Gu P, et al. Polypyrimidine Tract-Binding Protein 1 promotes proliferation, migration and invasion in clear-cell renal cell carcinoma by regulating alternative splicing of PKM. Am J Cancer Res 2017;7:245–59.
28. Yu F, Yao H, Zhu P, Zhang X, Pan Q, Gong C, et al. let-7 regulates self renewal and tumorigenicity of breast cancer cells. Cell 2007;131:1109–23.
29. Huang G, Wu X, Li S, Xu X, Zhu H, Chen X. The long noncoding RNA CASC2 functions as a competing endogenous RNA by sponging miR-18a in colorectal cancer. Sci Rep 2016;6:26524.
30. Salvador MA, Wicinski J, Cabaud O, Toiron Y, Finetti P, Josselin E, et al. The histone deacetylase inhibitor abexinostat induces cancer stem cells differentiation in breast cancer with low Xist expression. Clin Cancer Res 2013;19:6520–31.
31. Akrami R, Jacobsen A, Hoell J, Schultz N, Sander C, Larsson E. Comprehensive analysis of long non-coding RNAs in ovarian cancer reveals

global patterns and targeted DNA amplification. PLoS One 2013;8: e80306.
32. Siomi H, Matunis MJ, Michael WM, Dreyfuss G. The pre-mRNA binding K protein contains a novel evolutionarily conserved motif. Nucleic Acids Res 1993;21:1193–8.
33. Thisted T, Lyakhov DL, Liebhaber SA. Optimized RNA targets of two closely related triple KH domain proteins, heterogeneous nuclear ribonucleoprotein K and alphaCP-2KL, suggest distinct modes of RNA recognition. J Biol Chem 2001;276:17484–96.
34. Maenner S, Blaud M, Fouillen L, Savoye A, Marchand V, Dubois A, et al. 2-D structure of the A region of Xist RNA and its implication for PRC2 association. PLoS Biol 2010;8:e1000276.
35. He S, Zhang H, Liu H, Zhu H. LongTarget: a tool to predict lncRNA DNA-binding motifs and binding sites via Hoogsteen base-pairing analysis. Bioinformatics 2015;31:178–86.
36. Siegle JM, Basin A, Sastre-Perona A, Yonekubo Y, Brown J, Sennett R, et al. SOX2 is a cancer-specific regulator of tumour initiating potential in cutaneous squamous cell carcinoma. Nat Commun 2014;5:4511.
37. Guo W, Liu S, Cheng Y, Lu L, Shi J, Xu G, et al. ICAM-1-Related noncoding RNA in cancer stem cells maintains ICAM-1 expression in hepatocellular carcinoma. Clin Cancer Res 2016;22:2041–50.
38. Ulitsky I, Bartel DP. lincRNAs: genomics, evolution, and mechanisms. Cell 2013;154:26–46.
39. Klimek-Tomczak K, Wyrwicz LS, Jain S, Bomsztyk K, Ostrowski J. Characterization of hnRNP K protein-RNA interactions. J Mol Biol 2004;342: 1131–41.
40. Wen Y, Cai J, Hou Y, Huang Z, Wang Z. Role of EZH2 in cancer stem cells: from biological insight to a therapeutic target. Oncotarget 2017; 8:37974–90.
41. Lee SR, Roh YG, Kim SK, Lee JS, Seol SY, Lee HH, et al. Activation of EZH2 and SUZ12 regulated by E2F1 predicts the disease progression and aggressive characteristics of bladder cancer. Clin Cancer Res 2015;21:5391–403.
42. Huarte M, Guttman M, Feldser D, Garber M, Koziol MJ, Kenzelmann-Broz D, et al. A large intergenic noncoding RNA induced by p53 mediates global gene repression in the p53 response. Cell 2010;142:409–19.
43. Mondal T, Subhash S, Vaid R, Enroth S, Uday S, Reinius B, et al. MEG3 long noncoding RNA regulates the TGF-beta pathway genes through formation of RNA-DNA triplex structures. Nat Commun 2015;6:7743.
44. Arnold K, Sarkar A, Yram MA, Polo JM, Bronson R, Sengupta S, et al. Sox2 (+) adult stem and progenitor cells are important for tissue regeneration and survival of mice. Cell Stem Cell 2011;9:317–29.
45. Mukherjee P, Gupta A, Chattopadhyay D, Chatterji U. Modulation of SOX2 expression delineates an end-point for paclitaxel-effectiveness in breast cancer stem cells. Sci Rep 2017;7:9170.
46. Zhang Z, Duan Q, Zhao H, Liu T, Wu H, Shen Q, et al. Gemcitabine treatment promotes pancreatic cancer stemness through the Nox/ROS/NF-kappaB/STAT3 signaling cascade. Cancer Lett 2016;382:53–63.
47. Ooki A, Del Carmen Rodriguez Pena M, Marchionni L, Dinalankara W, Begum A, Hahn NM, et al. YAP1 and COX2 coordinately regulate urothelial cancer stem-like cells. Cancer Res 2018;78:168–81.
48. Zhu F, Qian W, Zhang H, Liang Y, Wu M, Zhang Y, et al. SOX2 is a marker for stem-like tumor cells in bladder cancer. Stem Cell Rep 2017;9:429–37.